J Appl Electrochem (2010) 40:39–47
DOI 10.1007/s10800-009-9961-8

ORIGINAL PAPER

The electrochemical corrosion behavior of sealed Ni–TiO_2 composite coating for sintered NdFeB magnet

Xiao-kui Yang · Qing Li · Jun-ying Hu · Xian-kang Zhong · Shi-yan Zhang

Received: 16 April 2009 / Accepted: 9 June 2009 / Published online: 21 June 2009

Abstract In this article, a protective sealed Ni–TiO_2 composite coating (SCC) was prepared on sintered NdFeB magnet by pulse current electrodeposition and sol–gel combined technique. For a comparison, unsealed Ni–TiO_2 composite coating (UCC) was also studied. The surface morphologies of composite coating were studied using scanning electron microscope (SEM). The structure of sealing layer was studied by Fourier transform infrared (FT-IR) spectrum. The anticorrosive properties of composite coating in neutral 3.5 wt% NaCl solution were evaluated by potentiodynamic polarization measurements and electrochemical impedance spectroscopy (EIS). In order to further investigate the anticorrosive properties of SCC, a long-term immersion test was carried out in neutral 3.5 wt% NaCl solution. The results of corrosion tests showed that due to the blocking effect of sealing layer, SCC can suppress the corrosion process by holding back the transfer or diffusion of corrosive medium, and therefore showed the excellent anticorrosive properties for sintered NdFeB magnet.

Keywords Ni–TiO_2 composite coating · Sintered NdFeB magnet · Sealing · Potentiodynamic polarization · Electrochemical impedance spectroscopy

Q. Li (✉) · J. Hu · X. Zhong · S. Zhang
School of Chemistry and Chemical Engineering, Southwest University, 400715 Chongqing, People's Republic of China
e-mail: liqingd@swu.edu.cn; liqingswu@yeah.net

X. Yang
School of Materials Science and Engineering, Southwest University, 400715 Chongqing, People's Republic of China

1 Introduction

The sintered NdFeB (neodymium–iron–boron) magnet, which was developed in the beginning of the 1980s, has been used for many applications in various fields such as acoustics, communications, and automation because of its excellent properties such as high remanence, high coercivity, and large energy product [1–3]. However, sintered NdFeB permanent magnets are highly vulnerable to the attack of corrosive environment, which impedes and limits their extensively wide applications [4, 5].

In order to improve the corrosion resistance of sintered NdFeB magnet, numerous attempts have been made, such as alloy additions and surface treatment [6–16], among which the electroplating of metal coatings is one of the most popular methods. As a traditional surface treatment technique, electroplating of metal coatings has been brought for surface modification of many metals, such as Al, Fe, NdFeB, Mg, etc. Composite electroplating is a method of codepositing fine particles of metallic, non-metallic compounds, or polymers in an electrodeposited metal matrix to improve material properties such as wear resistance, lubrication, or corrosion resistance in comparison with the single metal coatings [17]. Over the past few years, metal matrix composite coatings, especially nickel matrix composite coatings containing nano-particles which exhibit excellent properties, such as higher wear and corrosion resistance, higher hardness, and more excellent self-lubricating in comparison with single metal coating, have been more widely studied.

With the review and analysis of recent literatures on composite electrodeposition, it can be found that many research efforts with Al_2O_3, CeO_2, SiC, TiO_2, ZrO_2, and SiO_2, as the additive particles and with mild steel, stainless steel, copper, aluminum etc. as the substrate have been

widely reported [18–23]. However, pulse composite electrodeposition on sintered NdFeB magnet has not sa far been reported. In addition, it is well known that pulse electrodeposition is one of the most effective methods in fabrication of coatings due to its independently controllable parameters and higher instantaneous current density when compared to traditional direct current electrodeposition [24–26]. In addition, with the review of the literatures about the corrosion protection for sintered NdFeB magnet [6–16], it is also found that most of the literatures in relation to the corrosion protection for sintered NdFeB magnet focused on the test of short-term anticorrosive properties, but seldom the test of the long-term anticorrosive properties. Of the two, the latter is far better than the former to reflect the protective properties of coating for sintered NdFeB magnet.

In this study, pulse electrodeposited Ni–TiO_2 composite coating was successfully performed on sintered NdFeB magnet. In order to seal the surface defects and further improve the anticorrosive properties of Ni–TiO_2 composite coating, an effective sealing method using multi-immersion technique to add an organic sealing layer on Ni–TiO_2 composite coating had been developed. The effectiveness of sealed Ni–TiO_2 composite coating (SCC) on protective properties for sintered NdFeB magnet was evaluated by potentiodynamic polarization and electrochemical impedance spectroscopy (EIS). A systematic investigation in the anticorrosive properties of sealed Ni–TiO_2 composite coating (SCC) was carried out by EIS measurement in 3.5 wt% NaCl solution.

2 Experimental

2.1 Materials

Commercial powder-sintered NdFeB magnets for this investigation which were purchased from Shenzhen Dongsheng Magn. Mater. Co., Ltd, (China) were composed of 60.9% Fe, 28.6% Nd, 1.0% B, and other elements (in mass fraction). They were in disk form with diameter and thickness of 12.0 mm and 2.0 mm, respectively. Anatase TiO_2 powder was purchased from Shanghai CaiYu Nano technique Co., LTD, (China) with a mean diameter of 10 nm. A nickel plate with the purity of 99.99% was used as anode on the side of the electrolytic cell.

2.2 Pretreatment of magnet

Before electroplating, the substrate was sequentially polished with silicon carbide paper from grit #400 to #2000, rinsed with deionized water, ultrasonically degreased in an alkaline solution containing 70 g L^{-1} $Na_3PO_4 \cdot 12H_2O$, 50 g L^{-1} Na_2CO_3, 10 g L^{-1} NaOH, 0.5 g L^{-1} sodium dodecyl sulfate (SDS) and 0.5 g L^{-1} OP-10 (pH adjusted to 10–11 by formic acid) at 70 °C for 2 min, and then rinsed with hot and cold deionized water, respectively. In order to remove the oxidized film from the substrate, the above pretreated substrate was dipped into an acid solution containing 40 mL L^{-1} HNO_3 (65.0 wt%) and 0.5 g L^{-1} thiourea with the pH adjusted to 4–5 by ammonia, for approximately 10 s at room temperature. At last, the substrate was activated by the $PdCl_2$/EtOH solution containing 0.3–0.5 g L^{-1} with the pH of 7, for 2–5 s at room temperature.

2.3 Electrodeposition process

The Ni–TiO_2 composite coating was electrodeposited from a nickel Watts type bath. The optimized bath composition and other parameters obtained from large numbers of orthogonal experiments are given in Table 1.

2.4 Synthesis of sealing agent and sealing process

The sealing agent was Silica sol (Si sol) which was prepared using the following two-step process: (i) acid catalysis-based hydrolysis and (ii) alkaline catalysis-based condensation. Acetic acid (pH < 6) was initially introduced into the stirring mixture including tetraethyl orthosilicate (TEOS) and triethoxyvinylsilane (VTEO) (1.16 mol/L Si in ethanol and TEOS:VTEO in a 1:3 molar ratio) drop by drop at 60 °C, then stirred for 30 min; then, ammonia was introduced into the mixed solution drop by drop until the precursor was pH 7.0. Finally, the formed sol was aged for 1 day at room temperature before deposition on the Ni–TiO_2 composite coating.

Table 1 Bath compositions and operating conditions for pulse current electrodeposition

Bath composition and operating conditions	Quantity
$NiSO_4 \cdot 6H_2O$	260 g L^{-1}
$NiCl_2 \cdot 6H_2O$	42 g L^{-1}
H_3BO_3	36 g L^{-1}
Nano-TiO_2	10 g L^{-1}
SDS	0.1 g L^{-1}
Peak current density (J_p)	2 A dm^{-2}
Pulse frequency	100 Hz
Duty cycle	40%
pH	4.1
Temperature	50 °C
Time	40 min
Agitating	Continuous

The Si sol was employed as sealing agent, and the method of sealing adopted was dip-coating technique. After immersion in the sealing agent for about 3 min, the specimens were taken out and cured in an oven at 100 °C for 60 min. The process mentioned above was cycled two times for effectively sealing the microdefects on Ni–TiO_2 composite coating surface.

2.5 Tests

The Fourier transform-infrared (FT-IR) spectrum recorded with IR-10300 (America) was carried out to analyze the structure of Si sol. The microstructure and surface morphology of composite coating was characterized by a scanning electron microscope (SEM) S-4800 (HITACHI, Tokyo, Japan). The energy used for analysis was 20 kV.

The potentiodynamic polarization curves were performed by PS-268B system (Zhongfu, Beijing, China). A conventional three-electrode cell, with the specimens as the working electrode, a saturated calomel electrode (SCE) as reference, and a platinum sheet as counter electrode, were employed in those tests. Working electrode was embedded into epoxy resin with an exposure area of 1 cm^2. The specimens were immersed in the electrolyte for approximately 30 min prior to each test, allowing the system to be stabilized. The test electrolyte was neutral 3.5 wt% NaCl solution, and the test temperature was maintained at 30 °C. The potential was scanned from −1.1 V/SCE to 0.6 V with a scanning rate of 1 mV s^{-1}.

The electrochemical impedance spectroscopy (EIS) measurements were performed with CHI-660B system (Chenhua, China). The employed amplitude of sinusoidal signal was 5 mV, and the frequency range studied was from 10^5 to 10^{-2} Hz. The test electrolyte was neutral 3.5 wt% NaCl solution, and the test temperature was maintained at 30 °C. The specimens embedded into epoxy resin with an exposure area of 1 cm^2 were immersed in the solution for about 1 h before each test to establish the open circuit potential (E_{OCP}) or the steady state potential. The acquired data were curve fitted and analyzed using ZsimpWin 3.10 software.

The electrochemical corrosion tests mentioned above were normally repeated three times under the same conditions, checking that they presented reasonable reproducibility.

3 Results and discussions

3.1 SEM images analysis

The surface morphologies of sealed composite coating (SCC) and unsealed composite coating (UCC) are shown in Fig. 1. An irregular spherical crystal structure for UCC was observed as shown in Fig. 1a. A magnified scanning electron micrograph for UCC is presented in Fig. 1b. It can be seen from Fig. 1b that UCC was scraggly, and there were some pores on the surface with the result that corrosive medium, e.g., chloride ions, could easily conglomerate there and penetrate the coating through these pores resulting in the dissolution of metal coating over the pores and then the corrosion of the substrate. The surface morphology of SCC with a high magnification is shown in Fig. 1c. With the Si sol as sealing agent, the pores in the UCC were filled and overlaid because of which the transport of corrosive medium was held back, and therefore the corrosion process of coating was suppressed to a certain extent. This can be proved by potentiodynamic polarization measurements and electrochemical impedance spectroscopy (EIS), which would be discussed below.

3.2 FT-IR analysis

The FT-IR absorption spectrums of UCC and SCC are shown in Fig. 2a and b, respectively. Because the surface of UCC was scraggly and some pores were presented on the surface as shown in Fig. 1c, resulting in the influence of the CO_2 in the environment during measurement being large, the evident absorption peak of CO_2 was observed at 2368 cm^{-1} (Fig. 2a). The absorption peak around 670 cm^{-1} corresponding to the Ti–O stretching [27] was observed due to the existence of TiO_2 particles in composite coating, while this band was found to be weak due to the presence of CO_2 existing in the pores of UCC. It is known that the Si–O–Si has an asymmetric stretching mode in a wide region [28], and the location depends upon the nature of the bonding associated with it. In Fig. 2b, an obvious absorption peak, which presented at around 1106 cm^{-1} and was attributed to v_{as} (Si–O–Si), was observed. The absorption peak of CO_2 was very weak due to the flat and non-defect surface of SCC.

3.3 Corrosion analysis

3.3.1 Potentiodynamic polarization

The typical potentiodynamic polarization curves of the different specimens are presented in Fig. 3.

It can be seen from Fig. 3 that a passive region was observed for SCC, indicating that anodic reaction was inhibited to a certain extent with the increase of anodic potential. However, the passive region was not observed for the bare substrate and UCC which exhibited active dissolution without any distinctive transition to passivation within the range of anodic potential studied. In addition, SCC showed much lower anodic current

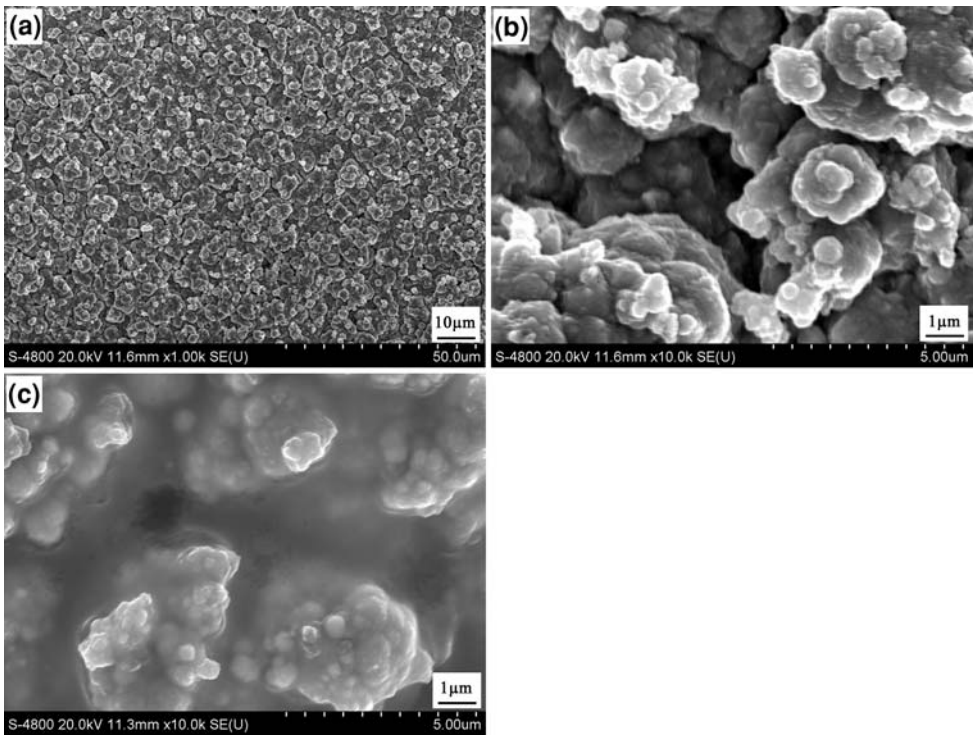

Fig. 1 SEM images of UCC (**a**, **b**) and SCC (**c**)

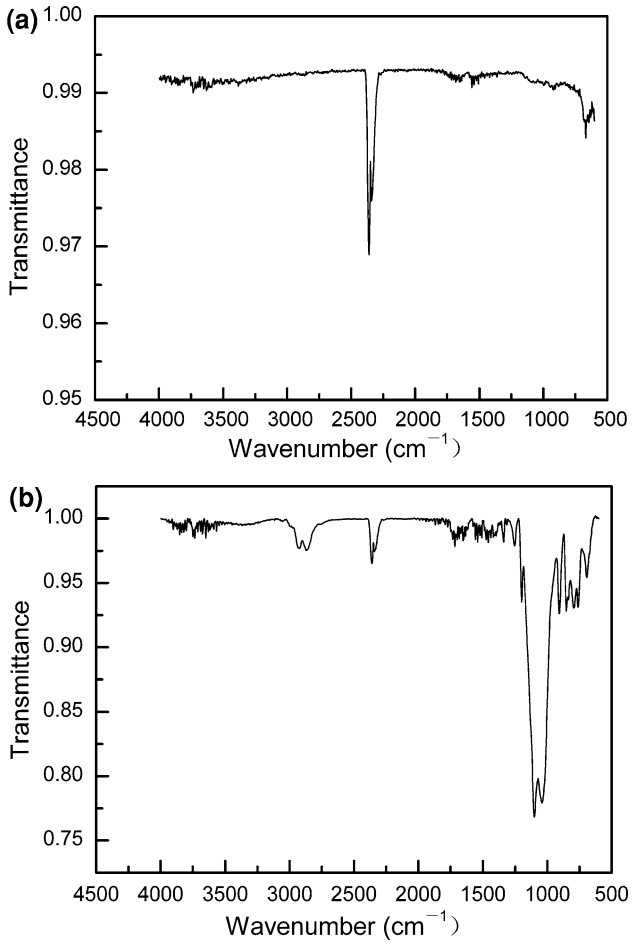

Fig. 2 The FT-IR spectrum of UCC (**a**) and SCC (**b**)

densities compared with UCC within the range of anodic potential studied, suggesting a lower corrosion rate.

Different parameters such as corrosion current density (I_{corr}), corrosion potential (E_{corr}), cathodic (β_c), and anodic (β_a) Tafel slopes derived from Fig. 3 using the PS-268B system are summarized in Table. 2. It can be seen that SCC exhibited the noblest E_{corr} with a value of -173 mV and the lowest I_{corr} with a value of 1.5×10^{-7} A cm^{-2}, while bare substrate showed the lowest E_{corr} with a value of -770 mV and the highest I_{corr} with a value of 4.6×10^{-6} A cm^{-2}, which suggested that SCC exhibited the best anticorrosive

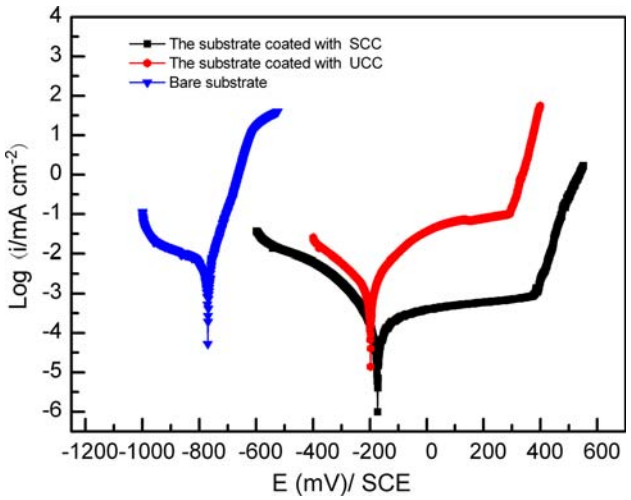

Fig. 3 The potentiodynamic polarization curves of different specimens in neutral 3.5 wt% NaCl solution

Table 2 Electrochemical parameters calculated from the potentiodynamic polarization curves

Specimens	E_{corr} (mV vs. SCE)	I_{corr} (A cm^{-2})	β_a (mV/decade)	β_c (mV/decade)
SCC	−173	1.5×10^{-7}	507	139
UCC	−198	2.1×10^{-6}	145	177
Substrate	−770	4.6×10^{-6}	39	344

properties. The E_{corr} and I_{corr} of UCC were measured to be −198 mV and 2.1×10^{-6} A cm^{-2}, respectively. It can be seen from Table 2 that the E_{corr} of SCC was slightly nobler than that of UCC, and the I_{corr} of SCC was approximately one-fourteenth of that of UCC which clearly showed that the corrosion rate of SCC decreased remarkably, and anticorrosive properties had been enhanced to a great extent due to the sealing treatment. From the analysis mentioned above, it can be seen that both SCC and UCC could provide excellent protection for the substrate, but nobler E_{corr} and much lower I_{corr} for the SCC indicated better protective properties provided for the substrate. In addition, the bare substrate had the lowest anodic Tafel slope (39 mV/decade), suggesting the fast active dissolution of substrate surface during polarization in 3.5% NaCl solution. The anodic Tafel slope of UCC (144 mV/decade) was distinctly higher than that for the bare substrate due to the lower electrochemical activity, while the anodic Tafel slope of SCC (506 mV/decade) markedly increased due to the blocking effect of the sealing layer.

The different polarization behaviors for SCC and UCC are mainly due to their different properties and structure. There were many defects and micropores on UCC surface (as shown in Fig. 1b). With the increase of anodic potential during polarization treatment, corrosive medium rapidly moved to these micropores and defects, and then congregated there under the action of electric field, resulting in the increase of the concentration of corrosive medium. When the polarization current reached certain value, the corrosive medium would rapidly react with UCC especially in these micropores and defects, resulting in the local preferential dissolution of coating, and then pits were formed. As regards SCC, due to the covering and blocking effect of sealing layer, transfer of corrosive medium was held back to a certain extent, and the increase of polarization current was suppressed during polarization treatment. Consequently, the corrosion process of SCC was slowed down, i.e., the anodic portion of the polarization curve of SCC showed the lower anodic current densities and higher anodic (β_a) Tafel slopes.

3.3.2 Electrochemical impedance spectroscopy

Impedance measurements are one of the most useful and informative methods for the corrosion assessment of metal coating and coated metals. They are capable of in situ and non-destructively probing relaxation phenomena over a wide frequency range [14].

The typical EIS plots displayed in Fig. 4 clearly shows the distinct differences among the different specimens. From the Bode plots (impedance modulus |Z| as a function of frequency), it can be seen that the impedance value of UCC increased by approximately three orders of magnitude compared with that of the bare substrate. The difference of impedance value between SCC and UCC cannot be well resolved from each other in the Bode plots (impedance modulus |Z| as a function of frequency) because no plateau at low frequency appeared in the frequency range studied. In order to further compare impedance value of SCC with

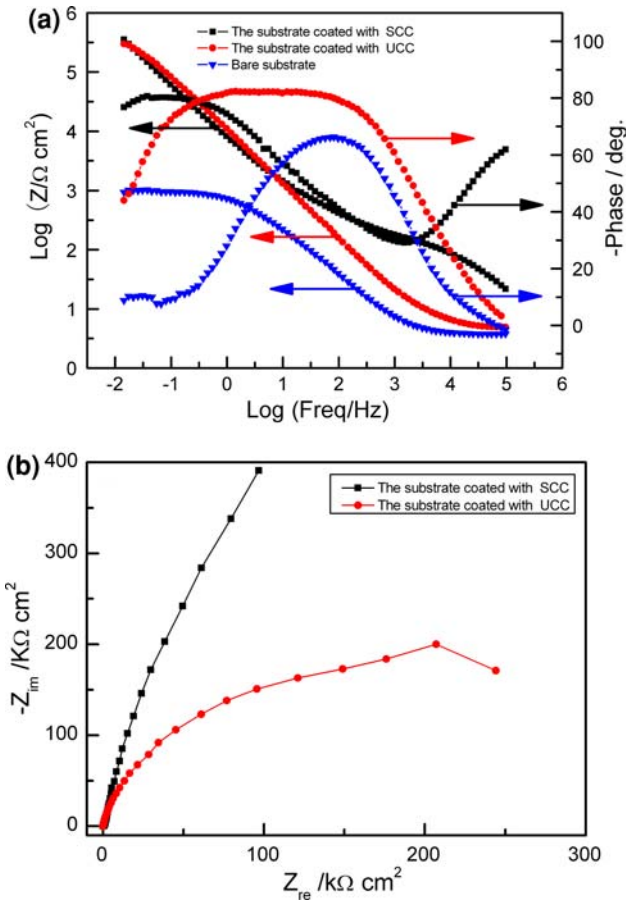

Fig. 4 The typical EIS plots of different specimens in neutral 3.5 wt% NaCl solution

that of UCC, the Nyquist plots for SCC and UCC are presented in Fig. 4b. It can be seen from Fig. 4b that the diameter of capacitance loop of SCC was larger than that of UCC indicating that SCC exhibited better anticorrosive properties compared with UCC. The changes in impedance phase angle (φ) indicated that there was only one time constant for the bare substrate and UCC over the whole frequency range studied which reflected one relaxation process (dissolution of working electrode during the corrosion process). The main difference between them was that UCC showed higher and much broader phase angle in comparison to bare substrate, also suggesting the improvement of anticorrosive properties of bare substrate after the pulse electrodeposition of UCC. The shape of the phase angle plot of SCC indicated the existence of three partially overlapped time constants which reflected three relaxation processes. The time constant in high-frequency range was associated with the existence of a protective sealing layer, another time constant was in the middle-frequency range, and the third one in low-frequency range could be attributed to the existence of Ni–TiO_2 composite coating. The physical meanings of the low-frequency and high-frequency range have been widely described [29–31], and the conclusion was very clear as stated above. Nevertheless, it is still worthwhile to discuss the origin of relaxation process in the middle-frequency range. Van Ooij's [29] and other group [30] who had studied the silane films on aluminum proposed that this time constant was attributed to the chemical formation of an "interfacial inorganic layer" between aluminum base and up-coated silane films. This layer may be composed of natural aluminum oxide and (or) Al–O–Si bonds. The Me–O–Si (Me stands for metals) structure has been detected in many silane-covered metals surface [31, 32]. In this case, the origin of relaxation process in the middle-frequency range may be ascribed to existence of the interfacial inorganic layer according to the studies mentioned above [29–32].

A more detailed interpretation of EIS measurement was performed by fitting the experimental plots using the electrochemical equivalent circuit depicted in Fig. 5. The electrochemical equivalent circuit displayed in Fig. 5a was proposed to account for the EIS data of bare substrate and UCC, while the circuit presented in Fig. 5b, for SCC. The circuit presented in Fig. 5a, consisted of parameters, namely, solution resistance (R_s), charge transfer resistance (R_{ct}), and a constant phase element (CPE) which replaced the capacitance of the double layer (C_{dl}). The CPE replaced the capacitance of the double layer (C_{dl}) due to the roughness and inhomogeneity of the electrode surface as reported elsewhere [19]. The circuit presented in Fig. 5b consisted of three RC circuits. The circuit $R_{po}CPE_0$ indicated the corrosion resistance of sealing layer corresponding to the high-frequency range of impedance

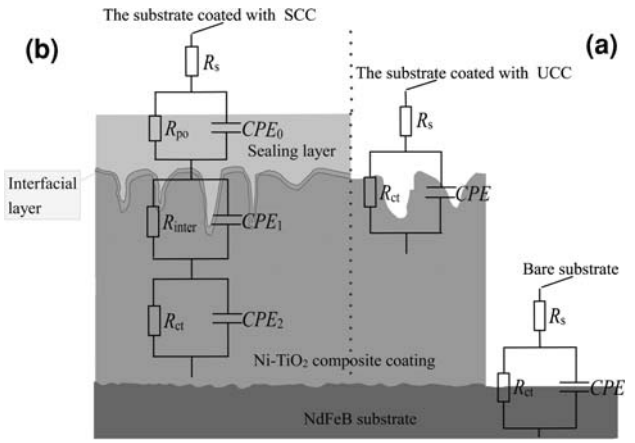

Fig. 5 Simplified schematic presentation of different specimens and the corresponding electrochemical equivalent circuits used for fitting the experimental data

spectroscopy. The circuit $R_{inter}CPE_1$ represented the corrosion process of interfacial layer corresponding to the middle-frequency range of impedance spectroscopy and $R_{ct}CPE_2$ described the electrode Faraday process (dissolution of Ni–TiO_2 composite coating) corresponding to the low-frequency range of impedance spectroscopy. The values of main circuit's element for the studied coating are listed in Table 3. It can be seen from Table 3 that the R_{ct} of UCC was $\sim$438 times higher than that of bare substrate which suggested excellent anticorrosive properties. After the sealing treatment on the UCC, the impedance value of SCC increased by more than one order of magnitude due to the blocking effect of the sealing layer.

In order to further study the protective properties of SCC for the substrate, the long-term immersion test in neutral 3.5 wt% NaCl solution has been carried out and electrochemical impedance spectroscopy analysis has been performed on the basis of Bode plots for selective immersion time.

Figure 6 shows the evolution of the impedance spectroscopy of SCC with different immersion times. It can be seen that the evolution of electrochemical corrosion behavior of SCC could be divided into three stages. The first stage was the immersion time ranging from 1 h to 240 h in which three partially overlapped time constants could be observed and the impedance modulus |Z| of SCC remains in a very high value, suggesting the excellent protective properties provided for the substrate. At the first stage, with the extension of immersion time, the impedance modulus |Z| of SCC fluctuated, but the differences among them were very slight. The second stage was the immersion time ranging from 240 h to 264 h in which two well-defined time constants could be observed, and the impedance modulus |Z| of SCC decreased sharply. At the second stage, the SCC still provided good protection for the

Table 3 Electrochemical parameters fitted from EIS measurement

Specimens	R_{po} (Ω cm^2)	Y_0 (Ω^{-1} cm^{-2} s^{-n})	n	R_{inter} (Ω cm^2)	Y_0 (Ω^{-1} cm^{-2} s^{-n})	n	R_{ct} (Ω cm^2)	Y_0 (Ω^{-1} cm^{-2} s^{-n})	n	Error |Z| (%)
SCC	1284	1.0×10^{-4}	0.8	102	1.3×10^{-6}	0.8	5.3×10^{6}	2.5×10^{-5}	0.9	4.8
UCC							4.4×10^{5}	1.8×10^{-5}	0.9	1.2
Substrate							1003	1.5×10^{-4}	0.8	1.3

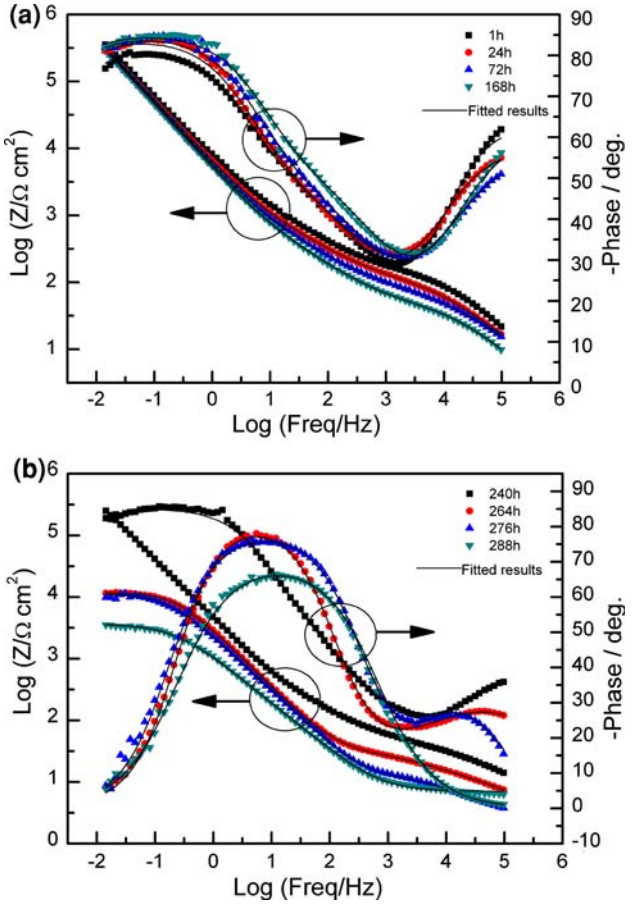

Fig. 6 Experimental and simulated Bode plots of SCC with different immersion time in neutral 3.5 wt% NaCl solution

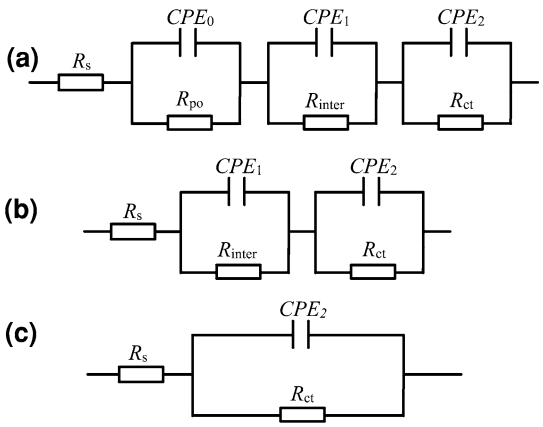

Fig. 7 Electrochemical equivalent circuits of SCC with different immersion times in neutral 3.5 wt% NaCl solution: **a** 1–240 h, **b** 240–264 h, and **c** 288 h

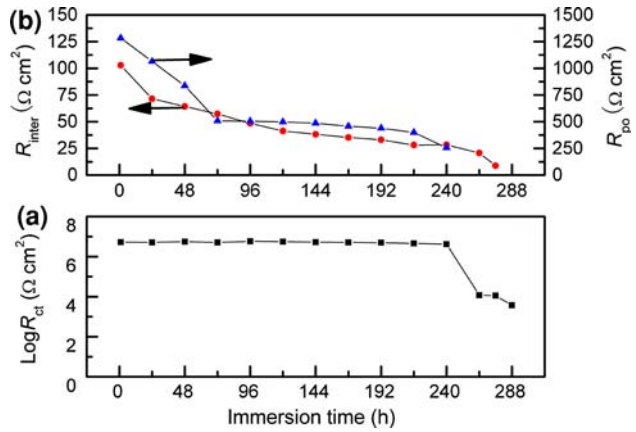

Fig. 8 The impedance values of different layers in SCC as a function of immersion time in neutral 3.5 wt% NaCl solution: **a** Ni–TiO_2 composite coating (R_{ct}); **b** sealing layer (R_{po}) and interfacial layer (R_{inter})

substrate. The third stage was the immersion time of 288 h in which only one well-defined time constant could be observed, and the impedance modulus |Z| of SCC decreased more, and then the protective properties of SCC for substrate practically disappeared.

The appropriate electrochemical equivalent circuits were proposed for further and quantitative analysis of the corrosion process of SCC with different immersion times (as shown in Fig. 7). The fitted results of EIS spectroscopy are presented in Fig. 8. Accordingly, the electrochemical corrosion behavior of SCC can be understood as follows. At the first hour of immersion, water and electrolyte passed through the diffusive pathway of sealing layer by diffusion, reached the interface between sealing layer and interfacial layer, and then the interface between interfacial layer and Ni–TiO_2 layer, reacting with the interfacial layer and Ni–TiO_2 composite coating with slow rate. At the moment, the SCC showed relatively high resistance as shown in Fig. 6a (1 h) and the impedance of sealing layer, interfacial layer, and Ni–TiO_2 composite coating showed the higher values as shown at the first point in Fig. 8. Owing to the covering and blocking effect of the sealing layer, transfer of corrosive medium, e.g., chloride ions, was held back to a

certain extent [33, 34]. As a result, the corrosion process of the Ni–TiO_2 composite coating was slowed down which may explain the slight fluctuation of R_{ct} before 240 h. The coating resistance (R_{po}) could reflect the anti-penetrating ability of Si sol, so it was used to evaluate the protective properties of sealing layer with the extension of immersion time. The changes of R_{po} with different immersion times indicated that the protective properties of Si sol gradually decreased with the increase of immersion time, which might be attributed to the fact that sealing layer suffered from a degradation process after exposure. The degradation process originated from the reason that the electrolyte penetrated the sealing layer and created more diffusive pathway to the underlying surface. The decrease in R_{inter} may reflect the fact that the electrolyte penetrated into the interfacial layer and consequently corrosion occurred in the interfacial region. With the immersion time of 240 h, because of the expansion of diffusive pathway, the corrosive medium easily passed through the Si sol, and then reacted with the interfacial layer and Ni–TiO_2 composite coating indicating that the disappearance of anticorrosive properties of sealing layer which corresponded to the disappearance of the first time constant. Consequently, with further increase of immersion time, corrosive medium would be rapidly transferred through interfacial layer due to the decreasing corrosion resistance, and congregated in the pores on the Ni–TiO_2 composite coating resulting in the rapid dissolution of Ni–TiO_2 composite coating which may be the main reason for the sharp decrease of R_{ct} with the immersion time of 264 h. With the immersion time of 288 h, the only one well-defined time constant appeared to indicate the disappearance of anticorrosive properties of the interfacial layer, and then the R_{ct} of Ni–TiO_2 composite coating decreased to $\sim 4000\ \Omega$ showing the last of protection by the coating.

4 Conclusions

In summary, the following conclusions have been drawn from the above investigation.

(1) A sealed Ni–TiO_2 composite coating (SCC), which markedly improved the corrosion resistance of sintered NdFeB magnet, was successfully applied on sintered NdFeB magnet by the combination of pulse current electrodeposition and the sol–gel method.

(2) Owing to the blocking effect of the sealing layer, the sealed Ni–TiO_2 composite coating (SCC) had much better corrosion resistance than that of unsealed Ni–TiO_2 composite coating (UCC). The values of corrosion current densities decreased by more than one order of magnitude, and the values of corrosion potential positively shifted by approximately 25 mV. Apart from pore plugging, the sealing layer enormously reduced the absorbent capacity of Ni–TiO_2 composite coating, preventing their degradation due to the penetration of corrosive substances from the environment.

(3) The long-term immersion test showed that the electrochemical corrosion behavior of sealed Ni–TiO_2 composite coating (SCC) could be divided into three stages. Owing to the blocking effect of sealing agent, sealed Ni–TiO_2 composite coating (SCC) could provide good protection for sintered NdFeB magnet in the course of immersion test.

Acknowledgments The authors acknowledge with thanks the financial supports granted by the Natural Science Foundation of Chongqing, China (CSTC. 2005BB4055), and the High-Tech Cultivation Program of Southwest Normal University (No. XSGX06).

References

1. Matsuura Y (2006) J Magn Magn Mater 303:344
2. Bai G, Gao RW, Sun Y, Han GB, Wang B (2007) J Magn Magn Mater 308:20
3. Vial F, Joly F, Nevalainen E, Sagawa M, Hiraga K, Park KT (2002) J Magn Magn Mater 242–245:1329
4. Cygan DF, McNallanm MJ (1995) J Magn Magn Mater 139:131
5. Rada M, Gebert A, Mazilu I, Khlopkov K, Gutfleisch O, Schultz L, Rodewald W (2006) J Alloys Compd 415:111
6. Tamborim Takeuchi SM, Azambuja DS, Saliba-Silva AM, Costa I (2006) Surf Coat Technol 200:6826
7. Yu LQ, Wen YH, Yan M (2004) J Magn Magn Mater 283:353
8. Walton A, Speight JD, Williams AJ, Harris IR (2000) J Alloys Compd 306:253
9. El-Moneim AA, Gebert A, Uhlemann M, Gutfleisch O, Schultz L (2002) Corros Sci 44:1857
10. Saliba-Silva A, Faria RN, Baker MA, Costa I (2004) Surf Coat Technol 185:321
11. Tamborim Takeuchi SM, Azambuja DS, Costa I (2006) Surf Coat Technol 201:3670
12. Man HH, Man HC, Leung LK (1996) J Magn Magn Mater 152:40
13. Cheng CW, Cheng FT (1998) J Appl Phys 83:6417
14. Hu JM, Liu XL, Zhang JQ, Cao CN (2006) Prog Org Coat 55:388
15. Song L, Wang Y, Lin W, Liu Q (2008) Surf Coat Technol 202:5146
16. Ma CB, Gao FH, Zhang Z, Zhang JQ (2006) Appl Surf Sci 253:2251
17. Low CTJ, Wills RGA, Walsh FC (2006) Surf Coat Technol 201:371
18. Szczygiel B, Kolodziej M (2005) Electrochim Acta 50:4188
19. Nowak P, Socha RP, Kaisheva M, Fransaer J, Celis JP, Stoinov Z (2000) J Appl Electrochem 30:429
20. Lin CS, Huang KC (2004) J Appl Electrochem 34:1013
21. Hu F, Chan KC (2004) Appl Surf Sci 233:163
22. Hou F, Wang W, Guo H (2006) Appl Surf Sci 252:3812
23. Li J, Sun Y, Sun X, Qiao J (2005) Surf Coat Technol 192:331
24. Wang W, Hou F, Wang H, Guo H (2005) Scripta Mater 53:613
25. Gyftou P, Pavlatou EA, Spyrellis N (2008) Appl Surf Sci 254:5910

26. Chen L, Wang L, Zeng Z, Xu T (2006) Surf Coat Technol 201: 599
27. Gurunathan K, Amalnerkar DP, Trivedi DC (2003) Mater Lett 57:1642
28. Bertelsen CM, Boerio FJ (2001) Prog Org Coat 41:239
29. Zhu D, Van Ooij W (2003) Cor Sci 45:2177
30. Zheludkevicha ML, Serra R, Montemor MF, Miranda Salvadoa IM, Ferreira MGS (2006) Surf Coat Technol 200:3084
31. Cabral A, Duarte RG, Montemor MF, Zheludkevich ML, Ferreira MGS (2005) Cor Sci 47:869
32. Ferreira MGS, Duarte RG, Montemor MF, Simões AMP (2004) Electrochim Acta 49:2927
33. Shang W, Chen B, Shi X, Chen Y, Xiao X (2009) J Alloys Compd 474:541
34. Tana ALK, Soutar AM, Annergrena IF, Liub YN (2005) Surf Coat Technol 198:478